Engineering xxx (xxxx) xxx

Contents lists available at ScienceDirect

Engineering

journal homepage: www.elsevier.com/locate/eng

Research
Textile Engineering–Article

Multifunctional, Wearable, and Wireless Sensing System via Thermoelectric Fabrics

Xinyang He [a], Jiaxin Cai [a], Mingyuan Liu [a], Xuepeng Ni [b], Wendi Liu [a], Hanyu Guo [a], Jianyong Yu [c], Liming Wang [a,*], Xiaohong Qin [a,*]

[a] Key Laboratory of Textile Science & Technology, Ministry of Education, College of Textiles, Donghua University, Shanghai 201620, China
[b] State Key Laboratory for Modification of Chemical Fibers and Polymer Materials, College of Materials Science and Engineering, Donghua University, Shanghai 201620, China
[c] Innovation Center for Textile Science and Technology, Donghua University, Shanghai 201620, China

ARTICLE INFO

Article history:
Available online xxxx

Keywords:
Thermoelectric fabrics
Wearable device
Wireless
Multifunctional sensing system
Outdoor wearable signal monitoring

ABSTRACT

Flexible thermoelectric materials play an important role in smart wearables, such as wearable power generation, self-powered sensing, and personal thermal management. However, with the rapid development of Internet of Things (IoT) and artificial intelligence (AI), higher standards for comfort, multifunctionality, and sustainable operation of wearable electronics have been proposed, and it remains challenging to meet all the requirements of currently reported thermoelectric devices. Herein, we present a multifunctional, wearable, and wireless sensing system based on a thermoelectric knitted fabric with over 600 $mm \cdot s^{-1}$ air permeability and a stretchability of 120%. The device coupled with a wireless transmission system realizes self-powered monitoring of human respiration through an mobile phone application (APP). Furthermore, an integrated thermoelectric system was designed to combine photothermal conversion and passive radiative cooling, enabling the characteristics of being powered by solar-driven in-plane temperature differences and monitoring outdoor sunlight intensity through the APP. Additionally, we decoupled the complex signals of resistance and thermal voltage during deformation under solar irradiation based on the anisotropy of the knitted fabrics to enable the device to monitor and optimize the outdoor physical activity of the athlete via the APP. This novel thermoelectric fabric-based wearable and wireless sensing platform has promising applications in next-generation smart textiles.

1. Introduction

Smart wearable devices have entered a new era. Through the processing of materials and the integration of devices, people can wear these devices anytime and anywhere, and these devices can accurately monitor multiple indicators of the human body in real time [1–4]. Among these indicators, the human physiological monitoring system shows great potential because it can help people monitor daily indicators such as breathing rate [5], skin temperature [6], human movement [7], rehabilitation exercise [8], and outdoor solar flux [9]. Therefore, the number of electronic devices is increasing, which in turn has increased the demand for intelligent terminals powered by traditional electrical energy systems. Wired charging systems are typically power sources whose bulky appearance, short lifespan, and potential toxicity hinder further development in smart wearables. Therefore, developing a new energy-harvesting technology that is easily accessible, efficient, and portable [10–15]. The human body and external environment generate a large amount of waste heat at all times, including body temperature, breathing temperature, sunlight, and so forth [16–18]. Thermoelectric materials can directly convert the temperature difference between the human body and external environment into electrical energy continuously, which is a good choice for wearable devices [19–24].

However, several challenges exist in the preparation and application of self-powered devices based on thermoelectric materials [25–31]. On the one hand, with the rapid increase in the integration of wearable devices, sensors with only a single temperature or strain sensing performance can no longer meet the needs of daily use [32,33]. For example, people are inevitably exposed to direct sunlight during outdoor activities. Therefore, it is reasonable to design a sunlight-based sensing system that can monitor human activity or help the body recognize the intensity of light to prevent

* Corresponding authors.
E-mail addresses: wangliming@dhu.edu.cn (L. Wang), xhqin@dhu.edu.cn (X. Qin).

https://doi.org/10.1016/j.eng.2023.05.026

Please cite this article as: X. He, J. Cai, M. Liu et al., Multifunctional, Wearable, and Wireless Sensing System via Thermoelectric Fabrics, Engineering, https://doi.org/10.1016/j.eng.2023.05.026

sunburn. It has been reported that sunlight is the most abundant outdoor resource, and if it is developed as the power source for thermoelectric-based self-powered devices, it is a breakthrough for wearable devices [34]. However, improving the wearability of thermoelectric materials to satisfy the comfort of daily human wear is still a major challenge [35,36]. Typically, flexible thermoelectric materials are made by blending a non-conductive elastomer with a thermoelectric material or by printing the thermoelectric material on a flexible substrate; this gives the material some flexibility but limits breathability, which prevents the transport of moisture from the skin to the outside, all of which lead to a poor wearing experience [37–41].

In addition, wireless configuration is another important advantage of sensor systems. Wireless sensing systems can eliminate the problem of built-in wire failure, are more portable, and are easy to install; therefore, they have been widely used in all aspects of human life [42–44]. However, multifunctional wearable wireless sensing systems based on thermoelectric materials have rarely been reported. Currently, the signals generated by thermoelectric-based sensors require a cable connection to a computer or multimeter for display and access, which hinders the integration of the entire system with everyday electronic devices.

In order to achieve multifunctionality and portability of the wearable product, we report a wireless sensing system based on thermoelectric fabrics (Fig. 1). N- and p-type thermoelectric fabrics were prepared by solution dip-coating method with excellent stretchability, breathability and durability to be used as the basic unit of the sensing system. The device composed of n- and p-type thermoelectric fabrics can be integrated with a wireless sensing module to monitor human breathing in real time via an application (APP) on a cell phone. In addition, a solar-flux monitoring device based on the photothermal effect and passive radiative cooling was fabricated by electrospinning a polyethylene oxide (PEO) nanofiber film directly onto one end of the device. The device enables round-the-clock solar flux monitoring with an app on the phone and solar-driven power harvesting. Furthermore, based on the structure of the stretching anisotropy of knitted fabrics, we decoupled the interference of resistance when the fabric was stretched and realized real-time monitoring of human joint movement in an outdoor sunlight environment. Overall, our wireless sensing system based on the fabric-based thermoelectrics offers a novel and effective strategy for developing next-generation wearable devices.

2. Materials and methods

2.1. Materials

Poly(3,4-ethylenedioxythiophene):poly(styrenesulfonate) (PEDOT:PSS) (1.3 wt% dispersion in H_2O; conductive grade) was purchased from Sigma-Aldrich Shanghai Trading Co., Ltd. (China). The carbon nanotube (CNT) dispersion (dispersed in water, single-walled, diameter of 1–2 nm) was purchased from Chengdu Organic Chemicals Co., Ltd., Chinese Academy of Sciences (China). Polyethylene oxide (PEO) (average Mv ~5 000 000; powder) and oleamine were obtained from Shanghai Aladdin Biochemical Technology Co., Ltd. (China). Commercially available cotton-knitted fabrics were also developed. Dimethyl sulfoxide (DMSO) and absolute ethanol (99.5%) were purchased from Sinopharm Chemical Reagent Co., Ltd. (China). All chemicals and materials were used as received without further purification.

2.2. Preparation of original thermoelectric fabric

Typically, the CNT dispersion was mixed with deionized water at a ratio of 1:1 using a cell crusher. The cotton-knitted fabrics with the same size were soaked in the homogeneous mixed dispersion for 1 h and dry at 40 °C. This procedure was repeated thrice. The obtained fabrics were then stirred violently in 80 °C deionized water to remove the residual organic matter and dry at 40 °C. This operation was repeated three times to obtain the original thermoelectric fabrics.

2.3. Preparation of p-type thermoelectric fabric

Firstly, 260 μL dimethyl sulfoxide (DMSO) was added into 5 mL of pristine PEDOT:PSS dispersion solution with ultrasonic dispersion for 1 h. Then thermoelectric fabrics were soaked in the obtained solution for 12 h, then dry in a vacuum at 40 °C. This operation was repeated three times to obtain p-type thermoelectric fabrics.

2.4. Preparation of n-type thermoelectric fabric

The original thermoelectric fabric exhibited typical p-type thermoelectric performance. To prepare the n-type thermoelectric fabrics, oleamine doping was performed according to previous reports [49]. Briefly, oleamine (2.5 mL) was mixed with of 23.0 mL and

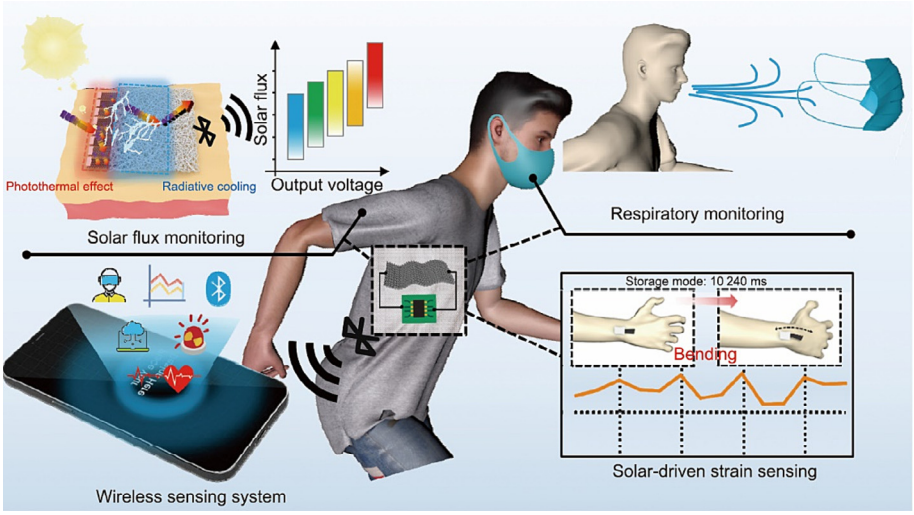

Fig. 1. Schematic and applications of the proposed wireless sensing system.

stirred vigorously for 2 h. The original thermoelectric fabrics were soaked in the mixed solution for 20 min and then dried to obtain the n-type thermoelectric fabrics.

2.5. Fabrication of thermoelectric device and solar flux monitoring device

Thermoelectric device for energy harvesting and sensing tests was composed of four p-type thermoelectric fabrics (1.5 cm × 0.5 cm) and four n-type thermoelectric fabrics (1.5 cm × 0.5 c m). Copper wires were used to connect the two types of fabrics, allowing the formation of one pair of p and n. Silver glue was added to reduce the contact resistance. The solar flux monitoring device was obtained by direct electrospinning of a PEO nanofiber film at one end of the prepared device. Written informed consent was obtained from all the participants.

2.6. Characterizations

The surface morphology and CNT state of the fabrics were characterized using field-emission (FE)-scanning electron microscopy (SEM) (Hitachi SU-8010; Hitachi, Ltd., Japan). The strain performance of the fabrics was tested using a universal material testing machine (25ST; Tinius Olsen Testing Machine Shanghai Co., Ltd., China). The air permeabilities of the fabrics were measured using a YG461G automatic air permeability measuring instrument. Absorption spectra were measured using an ultraviolet–visible-n ear-infrared (UV–Vis-NIR) spectrometer equipped with an integrating sphere (Shimadzu UV-3600; Shimadzu Corporation, Japan). The infrared (IR) (Nicolet 6700; Thermo Electron Corporation, USA) spectra were collected from 500 to 3500 cm^{-1}. Standard Air Mass (AM) 1.5G spectrum irradiation was performed using a solar simulator (CEL-FZ-A; Beijing Ceaulight Technology Co., Ltd., China). The thermal images of the samples were obtained using an IR camera (226; FOTRIC Intelligent Technology (Shanghai) Co., Ltd., China). The electrical conductivities and Seebeck coefficients of the thermoelectric fabrics were measured using a custom-built platform. Briefly, we placed a long composite film with dimensions of 20 mm × 5 mm on two Peltier elements for precise measurement. One of the Peltier elements was used for heating and the other was used for cooling to create a temperature difference. Temperature was monitored using an IR camera. The two probes were in direct contact with the silver glue at both ends of the composite film at a distance of 10 mm. A multimeter (Keithley 2400, USA) is used to measure the output voltage. The sensing signals of all devices were collected using a Keithley 2400 multimeter.

3. Results and discussions

3.1. Fabrication of breathable and stretchable thermoelectric fabrics

Fig. 2(a) illustrates the preparation of the breathable and stretchable thermoelectric fabrics. CNT were chosen as the base thermoelectric material because they have been reported to have excellent thermoelectric properties and can be easily modified to the p- or n-type using dopants. Cotton-knitted fabrics were chosen as substrates because of their good flexibility, stretchability, and breathability. Typically, the initial thermoelectric fabric is obtained by soaking a cotton-knitted fabric with a uniform shape in the obtained CNT dispersion. The obtained fabrics were extremely flexible and stretchable and could be sheared into any shape (Fig. S1 in Appendix A). The samples were placed on a self-built test platform to evaluate their thermoelectric properties (Fig. S2 in Appendix A). As shown in Fig. 2(a), the pristine CNT fabric possesses a positive Seebeck coefficient due to oxygen impurities, suggesting hole-like majority carriers [45–47]. Oleamine is reported to be a good n-dopant for converting CNT-based thermoelectrics to n-type materials that exhibit air stability [48,49]. The diameter of the pure CNT in Fig. S3(a) is smaller than the coating of oleamine on the CNT in Fig. S3(b) in Appendix A. Insulating oleamine led to a slight decrease in the conductivity of the fabric, but the Seebeck coefficient was compensated (Fig. 2(b)). In contrast, p-doping of the fabric resulted in a significant increase in the electrical conductivity of the fabric, which is similar to previous studies on CNT/PEDOT:PSS composites [50,51]. Comparing the CNT distribution patterns of the original fabric and the p-type fabric in Fig. S3(a) and (c) in Appendix A, it can be observed that the faintly visible fiber network produced by the PEDOT:PSS coating after the impregnation process indicates that PEDOT:PSS is well distributed on the fiber surface. At room temperature (T_0 = 24 °C), the temperature difference (ΔT) between the two ends of all the fabrics showed a good linear relationship with their output thermal voltage (Fig. S4(a) in Appendix A). In addition, the air stability of the n-type thermoelectric fabrics was measured to demonstrate the effectiveness of our doping strategy (Fig. S4(b)). Owing to the unique structure of knitted fabrics, they exhibit excellent air permeability [52]. As shown in Fig. 2(c), the air permeability of the doped fabric is slightly lower than that of the original cotton fabric, which can be attributed to the fact that the dopant reduces the pores between the fibers to a certain extent, while the pores between the yarns are retained because of the structure of the knitted fabric; thus, good air permeability is maintained. The yarn of the fabric was prepared using cotton fiber for good moisture absorption. As shown in Fig. S4(c) in Appendix A, the water drops on the fabric quickly wet the fabric, indicating that the thermoelectric fabric has good moisture absorption and can meet the body and external environment of water vapor exchange. Scanning electron microscopy (SEM) images of the two types of fabrics and single yarn are shown in Fig. S5 in Appendix A for additional explanation. Additionally, the mechanical properties of the fabric were tested to explore its potential use in wearable devices. As shown in Fig. 2(d), the strain values along the *Y*-direction for both the n- and p-type fabrics exceeded 130%, whereas the strain along the *X*-direction exceeded 190%, which is close to the values for cotton-knitted fabrics (Fig. S6 in Appendix A). It is worth noting that the direction along the coil is defined as the *Y*-direction. This indicates that the preparation process did not degrade the mechanical properties of the fabric.

Owing to its low cost, good processability, and high integratability, the fabric can be easily fabricated into large-area flexible thermoelectric devices. A flexible thermoelectric device composed of eight parallelly connected legs was fabricated using n-type fabrics as n-type legs, while p-type fabrics were used as p-type legs, as shown in Fig. 2(e). The internal resistance of the device was measured to be 980 Ω. In principle, the output voltage (U) of a thermoelectric device can be defined as $U = E - I{\cdot}R_{in}$, where E is the open-circuit voltage of the device, R_{in} is the internal resistance of the device, and I is the output current of the device. Therefore, the output current of the device is inversely proportional to the output voltage at a certain temperature difference. By connecting the device in series with an external load resistor, the output current − voltage curves are plotted for different temperature gradients (Fig. 2(f)). The current and voltage are inversely proportional, and the output voltage increases with the temperature difference. The output power (P) is calculated using the following expression: $P = E^2R_{load}/(R_{load} + R_{in})^2$, where R_{load} is the load resistance. When R_{in} and R_{load} are well matched ($R_{in} = R_{load}$), the maximum output power (P_{max}) of the device is obtained. As shown in Figs. 2(f) and (g), when the load resistance (R_{load}) is 980 Ω, the maximum output voltage and output power of the device can be obtained under different ΔT. Then, the device was worn directly on the wrist to assess its practical relevance as a wearable genera-

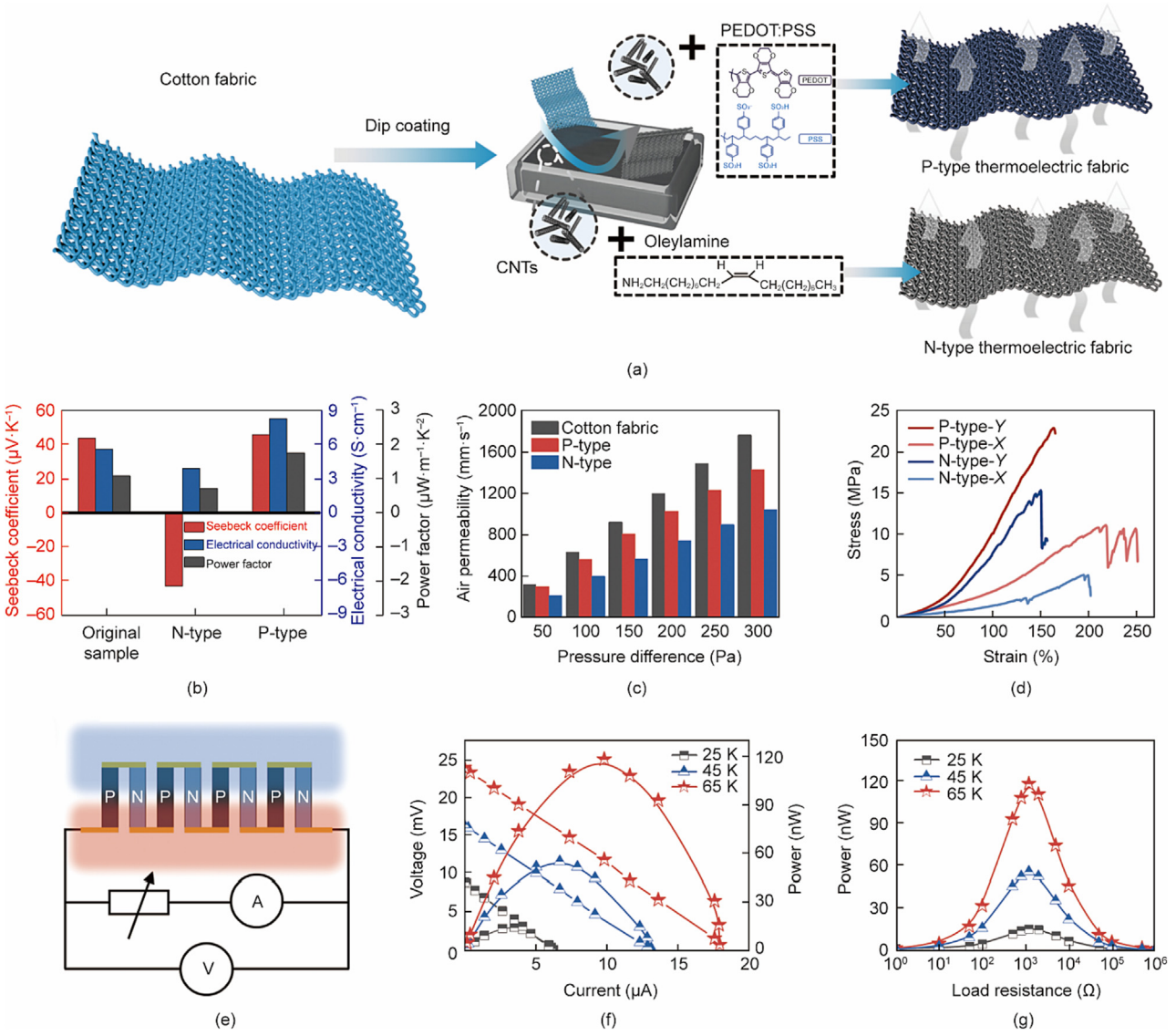

Fig. 2. (a) The fabrication process of p- and n-type thermoelectric fabrics. (b) Electrical conductivity, Seebeck coefficient, and power factor of the original thermoelectric fabrics, p- and n-type thermoelectric fabrics. (c) Air permeability of cotton fabrics, p- and n-type thermoelectric fabrics under different pressure. (d) Stress–strain curves of p- and n-type thermoelectric fabrics in different directions. (e) Schematic diagram of a thermoelectric device composed of four p-type thermoelectric fabrics (1.5 cm × 0.5 cm) and four n-type thermoelectric fabrics (1.5 cm × 0.5 cm) connected in series. (f) The relationship between the output voltage and output power versus the current of the device under different temperature differences. (g) The generated power of the device is a function of load resistance.

tor. As shown in Fig. S7(a) in Appendix A, one end of the device was in direct contact with the skin, and the other end was sewn to the fabric away from the skin to obtain a sufficient temperature difference. Fig. S7(b) shows that the temperature difference between the cold and hot ends of the device is approximately 3 K, and the device can produce a continuous output thermal voltage of 1.17 mV (Fig. S7(c)). These results reveal that our thermoelectric fabrics can be applied in the field of wearable energy harvesting.

3.2. Wireless temperature sensing via thermoelectric fabrics

The thermoelectric effect of the fabric allows it to perform temperature-sensing tests in self-powered mode at room temperature. It is well known that the minimum resolution temperature and discrimination between different temperatures of a temperature sensor are important metrics for evaluating its sensing performance [53]. Therefore, we performed a corresponding characterization using a p-type fabric as an example. We demonstrate its ability to detect a minimum temperature of 0.27 K (Fig. S8(a) in Appendix A). The ends of the sample were subjected to a small initial temperature difference, and the output thermal voltage was recorded in real time until the voltage started to change. The voltage at this point is the minimum output voltage, and then the temperature calculated at this point based on the functional relationship between the Seebeck coefficient and temperature ($\Delta T = \Delta V/S$) is defined as the minimum detection temperature.. The output thermal voltage corresponding to the temperature difference from 0 to 1 K for the n- and p-type fabrics is shown in Fig. S8(b) in Appendix A to illustrate the accuracy of the overall device. The ability to discriminate between the different temperature differences is shown in Fig. S8(c) in Appendix A. The cycling performance of a sensor is also an important metric. As shown in Fig. S8(d) in Appendix A, the device maintained stable sensing characteristics after 100 temperature-sensing cycles. Based on these characteristics, we integrated a flexible thermoelectric device consisting of eight parallel connected legs into a daily mask to monitor human breathing conditions. As shown in Fig. 3 (a), one end of the device was directly exposed to air, and the other

end was used for the inner measurement of the mouthpiece near the nose. The end exposed to air is always maintained at room temperature, whereas the temperature at the other end depends on the alternate inhalation and exhalation of the nose. As shown in the IR diagram, when we exhaled, the temperature measured inside the mouthpiece increased rapidly, the temperature difference from the ambient temperature increased rapidly, and the output thermal voltage of the device increased. When inhaled, airflow with ambient temperature entered the inside of the mouthpiece; the temperature at both ends of the device was at room temperature, and the output voltage rapidly decreased. Details of the thermal voltages generated by exhalation and inhalation are shown in Figs. S8(e) and (f) in Appendix A. As shown in Fig. 3(b), the thermal voltage generated by the device showed a regular rise and fall when breathing normally, dropped rapidly, and stabilized when breathing stopped. However, all the test data and results were obtained by plugging the device into a multimeter, which is not in line with the portability advocated for smart wearable devices.

Accordingly, we further integrated the device with a wireless circuit to construct a wireless respiratory detection system with bluetooth transmission, which is expected to be used for respiratory disease warning and respiratory arrest alarm (Figs. 3(c) and (d)). The operational principle of the wireless sensing system is described as follows: The voltage signal generated by the thermoelectric effect inside the sensor is collected by an analog-to-digital converter and sent to an operational amplifier. The signal is then analyzed by a microcontroller unit, which extracts the waveform, frequency, and period generated by the breath and sends the data in real-time to a mobile terminal via bluetooth. Notably, the sensor's signal is generated without any external power, by relying

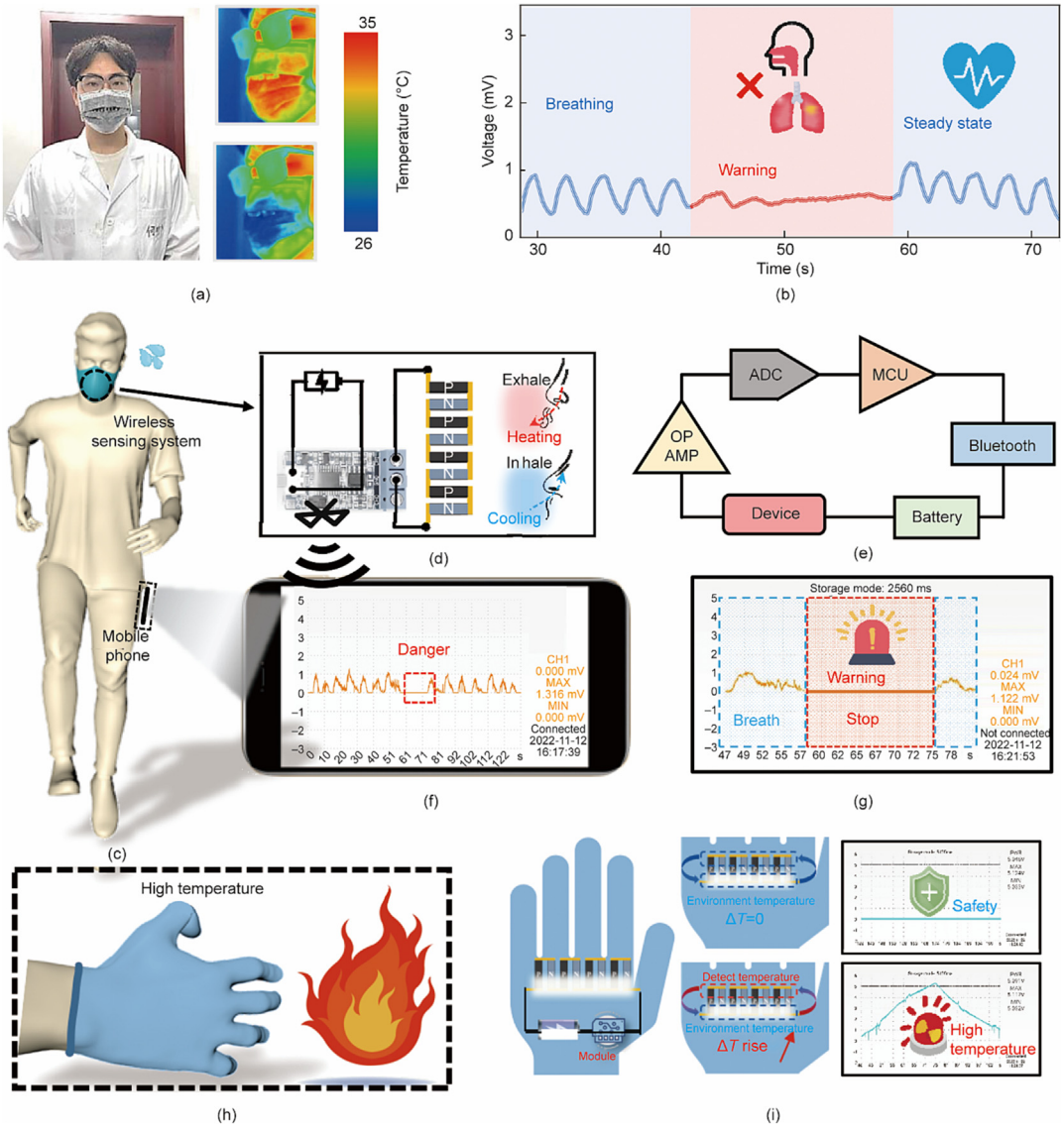

Fig. 3. (a) Physical diagram of the smart mask and the infrared images of exhalation and inhalation while wearing the mask. The device was integrated into the daily mask with one end directly exposed to the air and one end close to the nose. (b) The smart mask could detect the respiration by the change of thermal voltage when exhaling and inhaling. (c) Schematic diagram of the smart mask for respiratory monitoring. (d) Schematic image of the working principle of the wireless sensing system. (e) Schematic diagram of circuit principle of the wireless sensing system. (f) Real-time monitoring data of human breathing are monitored by wireless sensing systems and display the curve on a mobile phone APP. (g) The APP shows that the curve is regular when breathing and disappears into a straight line when stopping breathing. (h) Schematic diagram of smart gloves with high temperature warning capability. (i) Schematic and operational schematics of smart gloves with temperature detection capabilities. Real-time monitoring data was displayed on a mobile phone APP. ADC: analog to digital converter; MCU: microcontroller unit; OP AMP: operational amplifier.

only on the thermal voltage generated by its thermoelectric effect (Fig. 3(e)). As shown in Figs. 3(f) and (g), when the user is breathing normally, such as the time period from 0 to 60 s, the APP interface displays a regular curve change, which corresponds to the breathing activity of the human body. However, when the wearer stops breathing (i.e., the 60–70 s time period), the curve disappears, which implies that the user appears abnormal. A smart glove was also designed based on this system for temperature recognition and high-temperature detection (Fig. 3(h)). The sensor is integrated as shown in Fig. 3(i). When it does not touch the object, there is no temperature difference between the two ends of the sensor, and thus, no voltage signal is generated on the app. However, when it touches a hot object, the voltage curve on the app will rise rapidly. Thus, it can be used to monitor the touch temperature of the glove to ensure the safety of the user. In summary, our designed wireless sensing system based on thermoelectric fabric shows great potential in daily human safety protection such as breathing monitoring and high temperature warning.

3.3. Wireless solar-flux monitoring system based on solar-driven thermoelectric fabrics

In daily outdoor activities, the human body is often exposed to sunlight. Body temperature comfort will have an impact on the human body, and the high intensity of light can even harm the human skin. If we can monitor the intensity of sunlight in real time during the day and choose suitable clothes to resist the sunlight intensity, damage can be minimized. Sunlight has also been reported as a potential energy source for wearable devices and is widely used in various portable devices [54,55]. Based on this, we designed a wearable system based on a thermoelectric fabric to convert light into thermal voltage for real-time monitoring of solar flux during the day (Fig. 4(a)). One end of the device was covered with a PEO nanofiber film with a radiative cooling effect via direct electrostatic spinning (Fig. S9(a) in Appendix A), whereas the original device exhibited an excellent photothermal effect owing to the presence of CNT (Fig. S9(b) in Appendix A). The solar energy absorption capacities of the p- and n-type thermoelectric fabrics and PEO nanofiber films were tested and calculated. As shown in Fig. 4(b), the average absorption of both types of thermoelectric fabric was calculated to be higher than 90%, indicating that only 10% of the light was reflected or transmitted from the fabrics. This excellent solar energy harvesting capacity can be attributed to the superior thermal conversion efficiency of the CNT [56]. In contrast, the average absorption of the PEO nanofiber films was < 20%. PEO nanofiber films have been reported to achieve selective mid-IR radiation emission and effective sunlight reflection; thus, these films have excellent all-day radiative cooling properties [57]. SEM images of the PEO nanofiber films were also obtained to demonstrate the microscopic morphology of the fibers (Fig. S9(c) in Appendix A). To visualize the temperature change on both sides of the device under illumination and the generated output thermal voltage, the temperature response curves of the device under one-sun irradiation with time are shown in Fig. S10 in Appendix A. The

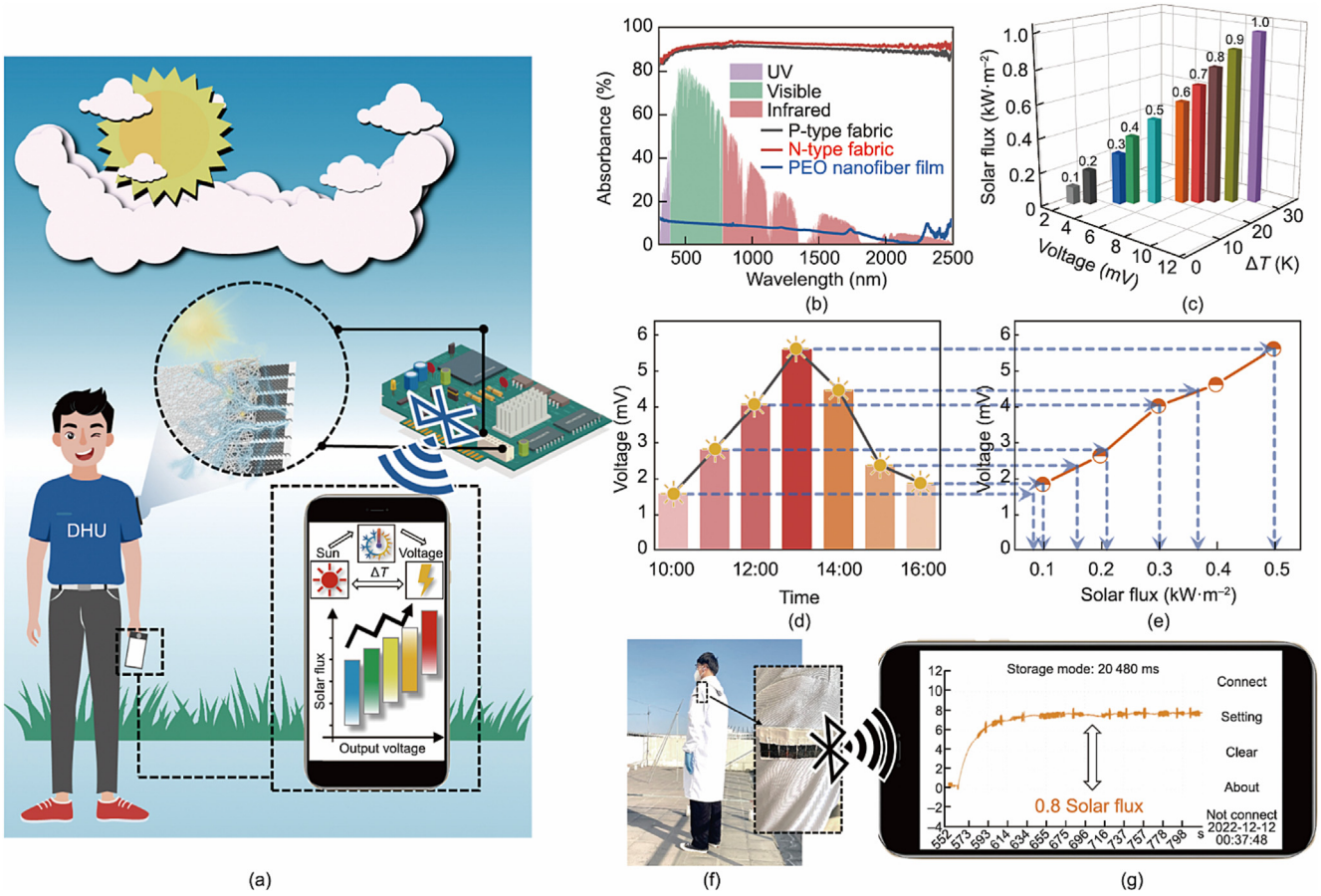

Fig. 4. (a) Schematic diagram of daytime solar flux monitoring system based on thermoelectric fabrics and its working principle diagram. (b) The absorption spectra of p-type thermoelectric fabric, n-type thermoelectric fabric, and PEO nanofiber film in the wavelength range from 300 to 2500 nm. (c) Temperature difference and voltage generated by devices under different sun fluxes. (d, e) Real-time voltage and corresponding solar flux of the device in an outdoor environment during the day. (f) Physical image of the device for solar flux monitoring. (g) Real-time monitoring data of solar flux was monitored by wireless sensing systems and displayed the curve on a mobile phone APP.

heating rate of the thermoelectric fabric was significantly higher than that of the PEO nanofiber film, and both reached a stable value after 150 s, producing a constant temperature difference of approximately 30 K (Fig. S11 in Appendix A).

The device can generate an output thermal voltage of about 9.5 mV (Fig. S12(a) in Appendix A), and the IR image of the device under one-sun irradiation is shown in Fig. S12(b) in Appendix A. This indicates a direct commutation relationship between the solar flux and the thermal voltage generated by the device. To validate the superiority of the device, the device without the PEO nanofiber film and that with paper were placed under one sun for comparison. As can be seen in Fig. S13 in Appendix A, the output thermal voltage of our device is much higher than that of the two comparison samples. This proves that our devices can establish stable and large in-plane temperature differences in the presence of sunlight. In addition, the cyclic repeatability of the device for solar flux is

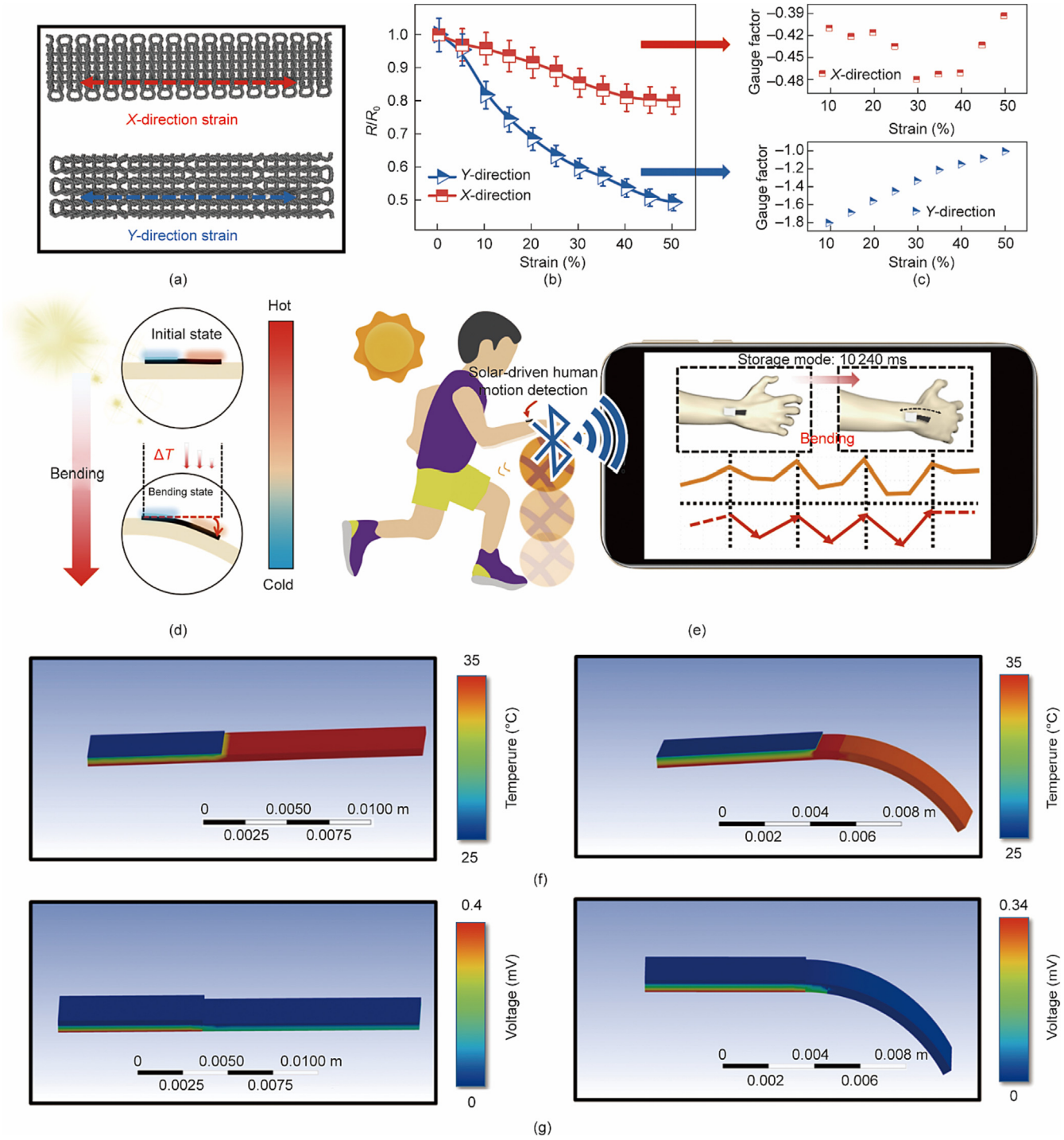

Fig. 5. (a) Schematic diagram of the thermoelectric fabric stretched in different directions. (b) Resistance response of the thermoelectric fabric in different directions. Fabric stretches in the *X*-direction to show better electrical stability. (c) GF of the thermoelectric fabric in different directions under different strains. (d) Schematic diagram of the change of ΔT at each end of the device when the wrist is bent under sunlight. (e) Real-time monitoring data of wrist bending was monitored by wireless sensing systems and displayed the curve on a mobile phone APP. (f) Simulation analysis of heat transfer before and after bending of the device under sunlight. (g) Simulation analysis of thermal voltage distribution before and after bending of the device under sunlight.

also demonstrated, as shown in Fig. S14 in Appendix A, and the test results of the integrated wireless sensing system are also shown in the mobile APP (Fig. S15 in Appendix A).

Further, the solar flux from 0.1 to 1 $kW \cdot m^{-2}$ corresponds to the thermal voltage generated by the device as shown in Fig. 4(c) to support the application prospects of the device for solar flux monitoring. The device was placed outdoors and exposed to direct sunlight to evaluate its practical significance in solar flux monitoring. Figs. 4(d) and (e) show the real-time solar fluxes and the corresponding open-circuit voltages generated at different time points during the day. Interestingly, this result corresponds to the daily variation in solar light; for example, light is the strongest between 12:00 and 1:00 pm. A device with integrated wireless circuitry was worn directly on the arm to monitor solar flux in real time in an outdoor environment (Fig. 4(f)). When the user stands in the sun, the mobile APP demonstrates a thermal voltage of about 0.8 mV, which corresponds to a solar flux of approximately 0.8 $kW \cdot m^{-2}$ (Fig. 4(g)). The above results show that the wireless solar flux monitoring system has practical implications for daytime solar flux monitoring and solar-driven thermoelectric energy harvesting and is expected to be used for early warning and real-time reporting of extreme weather.

3.4. Outdoor wireless human motion monitoring system based on the strain anisotropy thermoelectric knitted fabrics

With the excellent stretchability of thermoelectric fabrics and an energy supply design based on the photothermal effect and radiation cooling, they are expected to be used for the self-powered monitoring of human motion under outdoor solar illumination. The previously reported sensing mechanism of strain sensors based on self-powered thermoelectric materials is a change in the output thermal voltage caused by a change in the internal circuit during stretching [41,58]. However, under outdoor conditions, the stimulation source of the device not only comes from the thermal voltage reduction caused by human movement but also has to consider the irregular temperature difference caused by sunlight, and the two signals interfere with each other, making it difficult to properly monitor human motions.

Knitted fabrics with a unique structure that exhibited anisotropy in resistance changes when stretched along different directions were selected to solve this problem (Fig. 5(a)). First, the change in the resistance of the thermoelectric fabric when stretched along different directions was analyzed. It is worth noting that the self-powered strain sensors mentioned below are all made from p-type fabrics. As shown in Fig. 5(b), the resistance exhibited a negative response when the fabric was stretched along the *Y*-direction, whereas the change in resistance along the *X*-direction was not significant. A simple strain–resistance model was designed to understand the relationship between structural deformation and relative resistance changes during fabric stretching. Fig. S16 in Appendix A shows that the fabric model undergoes two stages of change when stretched along either the *X*- or *Y*-direction, first microscopically as a contraction of the yarn structure and then macroscopically as a contact of adjacent coils. When stretched along the *Y*-direction, there were more adjacent contact points, resulting in a significant negative resistance response. However, when stretched along the *X*-direction, the resistance remained relatively stable even when the strain reached 50%. More intuitive strain-insensitive properties are shown in Fig. 5(c) for the gauge factor (GF). SEM images of the fabric before and after stretching along the *X*- and *Y*-directions are shown in Fig. S17 in Appendix A for additional illustration. In addition, the change in resistance over 100 strain cycles was tested to determine the durability of the fabric (Fig. S18 in Appendix A).

Therefore, the *X*-direction of the fabric was chosen as the tensile direction, and one end of the fabric was electrospun with PEO nanofiber films to fabricate a strain sensor that could be mounted on wrist for human motion detection (Fig. S19 in Appendix A). Corresponding to the strain-insensitive property of the fabrics, the resistance of the sensor remains stable when bending. The device was tested by mounting on wrist and subsequently bending the wrist in an outdoor solar environment. In the initial state, the device generated a thermal voltage of approximately 0.4 mV (Fig. S20 in Appendix A), which corresponded to the Seebeck coefficient of the device, and the thermal voltage decreased upon bending (Fig. S21 in Appendix A). It was previously concluded that the internal circuitry of the device is not affected by the strain deformation; thus, the source of stimulation is the reduced temperature difference between the two ends of the device, and this reduced temperature difference is caused by insufficient illumination due to bending (Fig. 5(d)). Further, the sensor was integrated into the wireless transmission system and was used to monitor the training metrics of the athletes in an outdoor environment, such as recording basketball players' dribble counts. The data and graphs shown in the APP were consistent with the results of the previous tests (Fig. 5(e)). In addition, the heat transfer mechanism and thermal voltage dispersion of the device before and after bending under sunlight were simulated and analyzed to corroborate the conclusions (Figs. 5(f) and (g)). The simulation results show that the temperature of the hot end after bending is significantly lower than that before bending and results in thermal voltage drop, which is consistent with our test results and indicates the advanced nature of our structural design.

4. Conclusions

In summary, an original multifunctional wearable wireless sensing system based on a thermoelectric knit fabric was proposed. The thermoelectric fabric exhibited a good air permeability of over 600 $mm \cdot s^{-1}$ at 100 Pa, over 120% strain, and a precise temperature recognition of 0.27 K. A wireless Bluetooth module was integrated with a fabric-based thermoelectric device to successfully monitor human respiration using a mobile phone APP. Moreover, the wireless sensing system was expanded to detect outdoor sunlight intensity, predict extreme weather, and monitor motion in real time under outdoor sunlight conditions to improve sports performance by constructing a solar-driven in-plane thermoelectric device that combines photothermal conversion and passive radiative cooling effects. The sensing platform reported herein provides a novel idea for the development of multifunctional wearable electronics.

CRediT authorship contribution statement

Xinyang He: Conceptualization, Methodology. **Jiaxin Cai:** Conceptualization, Methodology. **Mingyuan Liu:** Methodology. **Xuepeng Ni:** Methodology. **Wendi Liu:** Validation. **Hanyu Guo:** Methodology. **Jianyong Yu:** Resources. **Liming Wang:** Resources, Conceptualization, Supervision. **Xiaohong Qin:** Resources, Supervision.

Acknowledgments

This work was partly supported by National Natural Science Foundation of China (51973027 and 52003044) , the Fundamental Research Funds for the Central Universities (2232020A-08), International Cooperation Fund of Science and Technology Commission of Shanghai Municipality (21130750100), and Major Scientific and Technological Innovation Projects of Shandong Province

(2021CXGC011004). This work has also been supported by the Chang Jiang Scholars Program and the Innovation Program of Shanghai Municipal Education Commission (2019-01-07-00-03-E00023) to Prof. Xiaohong Qin, State Key Laboratory for Modification of Chemical Fibers and Polymer Materials (KF2216) and Donghua University (DHU) Distinguished Young Professor Program to Prof. Liming Wang, and the Fundamental Research Funds for the Central Universities and Graduate Student Innovation Fund of Donghua University (CUSF-DH-D-2022040) to Xinyang He.

Compliance with ethics guidelines

Xinyang He, Jiaxin Cai, Mingyuan Liu, Xuepeng Ni, Wendi Liu, Hanyu Guo, Jianyong Yu, Liming Wang, and Xiaohong Qin declare that they have no conflict of interest or financial conflicts to disclose.

Appendix A. Supplementary data

Supplementary data to this article can be found online at https://doi.org/10.1016/j.eng.2023.05.026.

References

[1] Dubal DP, Chodankar NR, Kim DH, Gomez-Romero P. Towards flexible solid-state supercapacitors for smart and wearable electronics. Chem Soc Rev 2018;47(6):2065–12029.
[2] Gao W, Emaminejad S, Nyein HYY, Challa S, Chen KV, Peck A, et al. Fully integrated wearable sensor arrays for multiplexed in situ perspiration analysis. Nature 2016;529(7587):509–14.
[3] Lee J, Kwon H, Seo J, Shin S, Koo JH, Pang C, et al. Conductive fiber-based ultrasensitive textile pressure sensor for wearable electronics. Adv Mater 2015;27(15):2433–9.
[4] Oh JY, Rondeau-Gagné S, Chiu YC, Chortos A, Lissel F, Wang GN, et al. Intrinsically stretchable and healable semiconducting polymer for organic transistors. Nature 2016;539(7629):411–5.
[5] Güder F, Ainla A, Redston J, Mosadegh B, Glavan A, Martin TJ, et al. Paper-based electrical respiration sensor. Angew Chem Int Ed Engl 2016;55(19):5727–32.
[6] Hua Q, Sun J, Liu H, Bao R, Yu R, Zhai J, et al. Skin-inspired highly stretchable and conformable matrix networks for multifunctional sensing. Nat Commun 2018;9(1):244.
[7] Cheng Y, Wang RR, Sun J, Gao L. A stretchable and highly sensitive graphene-based fiber for sensing tensile strain, bending, and torsion. Adv Mater 2015;27(45):7365–71.
[8] Shao W, Zhang L, Jiang Z, Xu M, Chen Y, Li S, et al. Bioinspired conductive structural color hydrogels as a robotic knuckle rehabilitation electrical skin. Nanoscale Horiz 2022;7(11):1411–7.
[9] Yun SN, Qin Y, Uhl AR, Vlachopoulos N, Yin M, Li DD, et al. New-generation integrated devices based on dye-sensitized and perovskite solar cells. Energ Environ Sci 2018;11(3):476–526.
[10] Chen C, Jiang M, Luo X, Tai H, Jiang Y, Yang M, et al. Ni-Co-P hollow nanobricks enabled humidity sensor for respiratory analysis and human-machine interfacing. Sens Actuators B Chem 2022;370:132441.
[11] Guan H, Yang R, Li W, Tao Y, Chen C, Tai H, et al. Self-powered multifunctional flexible sensor for wearable biomonitoring. Sens Actuators B Chem 2023;377:132996.
[12] Pan H, Chen G, Chen Y, Di Carlo A, Mayer MA, Shen S, et al. Biodegradable cotton fiber-based piezoresistive textiles for wearable biomonitoring. Biosens Bioelectron 2023;222:114999.
[13] Su Y, Chen S, Liu B, Lu H, Luo X, Chen C, et al. Maxwell displacement current induced wireless self-powered gas sensor array. Mater Today Phys 2023;30:100951.
[14] Su Y, Li W, Cheng X, Zhou Y, Yang S, Zhang X, et al. High-performance piezoelectric composites via β phase programming. Nat Commun 2022;13(1):4867.
[15] Su Y, Liu Y, Li W, Xiao X, Chen C, Lu H, et al. Sensing-transducing coupled piezoelectric textiles for self-powered humidity detection and wearable biomonitoring. Mater Horiz 2023;10(3):842–51.
[16] Xue H, Yang Q, Wang DY, Luo WJ, Wang WQ, Lin MS, et al. A wearable pyroelectric nanogenerator and self-powered breathing sensor. Nano Energy 2017;38:147–54.
[17] Cao M, Wang X, Cao W, Fang X, Wen B, Yuan J. Thermally driven transport and relaxation switching self-powered electromagnetic energy conversion. Small 2018;14(29):1800987.
[18] Panwar NL, Kaushik SC, Kothari S. Role of renewable energy sources in environmental protection: a review. Renew Sustain Energy Rev 2011;15(3):1513–24.
[19] Shi XL, Zou J, Chen ZG. Advanced thermoelectric design: from materials and structures to devices. Chem Rev 2020;120(15):7399–515.
[20] Wang L, Zhang Z, Liu Y, Wang B, Fang L, Qiu J, et al. Exceptional thermoelectric properties of flexible organic-inorganic hybrids with monodispersed and periodic nanophase. Nat Commun 2018;9(1):3817.
[21] Zheng ZH, Shi XL, Ao DW, Liu WD, Li M, Kou LZ, et al. Harvesting waste heat with flexible Bi_2Te_3 thermoelectric thin film. Nat Sustain 2023;6(2):180–91.
[22] Zhao LD, Dravid VP, Kanatzidis MG. The panoscopic approach to high performance thermoelectrics. Energ Environ Sci 2014;7(1):251–68.
[23] Wang LM, Zhang ZM, Geng LX, Yuan TY, Liu YC, Guo JC, et al. Solution-printable fullerene/TiS_2 organic/inorganic hybrids for high-performance flexible n-type thermoelectrics. Energ Environ Sci 2018;11(5):1307–17.
[24] Zhao LD, Tan G, Hao S, He J, Pei Y, Chi H, et al. Ultrahigh power factor and thermoelectric performance in hole-doped single-crystal SnSe. Science 2016;351(6269):141–4.
[25] He X, Gu J, Hao Y, Zheng M, Wang L, Yu J, et al. Continuous manufacture of stretchable and integratable thermoelectric nanofiber yarn for human body energy harvesting and self-powered motion detection. Chem Eng J 2022;450:137937.
[26] Suarez F, Nozariasbmarz A, Vashaee D, Ozturk MC. Designing thermoelectric generators for self-powered wearable electronics. Energy Environ Sci 2016;9(6):2099–113.
[27] Zhang FJ, Zang YP, Huang DZ, Di CA, Zhu DB. Flexible and self-powered temperature-pressure dual-parameter sensors using microstructure-frame-supported organic thermoelectric materials. Nat Commun 2015;6:8356.
[28] He XY, Shi J, Hao YN, He MT, Cai JX, Qin XH, et al. Highly stretchable, durable, and breathable thermoelectric fabrics for human body energy harvesting and sensing. Carbon Energy 2022;4(4):621–32.
[29] Wan K, Liu Y, Santagiuliana G, Barandun G, Taroni Junior P, Güder F, et al. Self-powered ultrasensitive and highly stretchable temperature-strain sensing composite yarns. Mater Horiz 2021;8(9):2513–9.
[30] Kim CS, Yang HM, Lee J, Lee GS, Choi H, Kim YJ, et al. Self-powered wearable electrocardiography using a wearable thermoelectric power generator. ACS Energy Lett 2018;3(3):501–7.
[31] Kim SJ, We JH, Cho BJ. A wearable thermoelectric generator fabricated on a glass fabric. Energ Environ Sci 2014;7(6):1959–65.
[32] Liu ZK, Li ZH, Yi YPQ, Li LDN, Zhai H, Lu ZH, et al. Flexible strain sensing percolation networks towards complicated wearable microclimate and multi-direction mechanical inputs. Nano Energy 2022;99:107444.
[33] Jayathilaka WADM, Qi K, Qin Y, Chinnappan A, Serrano-García W, Baskar C, et al. Significance of nanomaterials in wearables: a review on wearable actuators and sensors. Adv Mater 2019;31(7):e1805921.
[34] Hyder F, Sudhakar K, Mamat R. Solar PV tree design: a review. Renew Sustain Energy Rev 2018;82:1079–96.
[35] Lama J, Yau A, Chen GR, Sivakumar A, Zhao X, Chen J. Textile triboelectric nanogenerators for self-powered biomonitoring. J Mate Chem A 2021;9(35):19149–78.
[36] Kim J, Byun S, Lee S, Ryu J, Cho S, Oh C, et al. Cost-effective and strongly integrated fabric-based wearable piezoelectric energy harvester. Nano Energy 2020;75:104992.
[37] Zhao YL, Cheng HL, Li YX, Rao JC, Yue SZ, Le QJ, et al. Quasi-solid conductive gels with high thermoelectric properties and high mechanical stretchability consisting of a low cost and green deep eutectic solvent. J Mate Chem A 2022;10(8):4222–9.
[38] Fang YL, Cheng HL, He H, Wang S, Li JM, Yue SZ, et al. Stretchable and transparent ionogels with high thermoelectric properties. Adv Funct Mater 2020;30(51):2004699.
[39] He X, Hao Y, He M, Qin X, Wang L, Yu J. Stretchable thermoelectric-based self-powered dual-parameter sensors with decoupled temperature and strain sensing. ACS Appl Mater Interfaces 2021;13(50):60498–507.
[40] Zhang D, Zhang KW, Wang YM, Wang YH, Yang Y. Thermoelectric effect induced electricity in stretchable graphene-polymer nanocomposites for ultrasensitive self-powered strain sensor system. Nano Energy 2019;56:25–32.
[41] Taroni PJ, Santagiuliana G, Wan K, Calado P, Qiu M, Zhang H, et al. Toward stretchable self-powered sensors based on the thermoelectric response of PEDOT:PSS/polyurethane blends. Adv Funct Mater 2018;28(15):1704285.
[42] Lim HR, Kim HS, Qazi R, Kwon YT, Jeong JW, Yeo WH. Advanced soft materials, sensor integrations, and applications of wearable flexible hybrid electronics in healthcare, energy, and environment. Adv Mater 2020;32(15):e1901924.
[43] Ray TR, Choi J, Bandodkar AJ, Krishnan S, Gutruf P, Tian L, et al. Bio-integrated wearable systems: a comprehensive review. Chem Rev 2019;119(8):5461–533.
[44] Liu Y, Pharr M, Salvatore GA. Lab-on-skin: a review of flexible and stretchable electronics for wearable health monitoring. ACS Nano 2017;11(10):9614–35.
[45] Yu CH, Murali A, Choi KW, Ryu Y. Air-stable fabric thermoelectric modules made of N- and P-type carbon nanotubes. Energ Environ Sci 2012;5(11):9481–6.
[46] Nonoguchi Y, Nakano M, Murayama T, Hagino H, Hama S, Miyazaki K, et al. Simple salt-coordinated n-Type nanocarbon materials stable in air. Adv Funct Mater 2016;26(18):3021–8.
[47] Collins PG, Bradley K, Ishigami M, Zettl A. Extreme oxygen sensitivity of electronic properties of carbon nanotubes. Science 2000;287(5459):1801–4.
[48] Wu G, Zhang ZG, Li Y, Gao C, Wang X, Chen G. Exploring high-performance n-Type thermoelectric composites using amino-substituted rylene dimides and carbon nanotubes. ACS Nano 2017;11(6):5746–52.

[49] Sun T, Zhou B, Zheng Q, Wang L, Jiang W, Snyder GJ. Stretchable fabric generates electric power from woven thermoelectric fibers. Nat Commun 2020;11(1):572.
[50] Kim JY, Lee W, Kang YH, Cho SY, Jang KS. Wet-spinning and post-treatment of CNT/PEDOT:PSS composites for use in organic fiber-based thermoelectric generators. Carbon 2018;133:293–9.
[51] Kim D, Kim Y, Choi K, Grunlan JC, Yu C. Improved thermoelectric behavior of nanotube-filled polymer composites with poly(3,4-ethylenedioxythiophene) poly(styrenesulfonate). ACS Nano 2010;4(1):513–23.
[52] Onofrei E, Rocha AM, Catarino A. The influence of knitted fabrics' structure on the thermal and moisture management properties. J Eng Fibers Fabrics 2011;6(4):10–22.
[53] Park J, Kim M, Lee Y, Lee HS, Ko H. Fingertip skin-inspired microstructured ferroelectric skins discriminate static/dynamic pressure and temperature stimuli. Sci Adv 2015;1(9):e1500661.
[54] Lee YH, Kim JS, Noh J, Lee I, Kim HJ, Choi S, et al. Wearable textile battery rechargeable by solar energy. Nano Lett 2013;13(11):5753–61.
[55] Bonaccorso F, Colombo L, Yu G, Stoller M, Tozzini V, Ferrari AC, et al. Graphene, related two-dimensional crystals, and hybrid systems for energy conversion and storage. Science 2015;347(6217):1246501.
[56] Song J, Wang F, Yang X, Ning B, Harp MG, Culp SH, et al. Gold nanoparticle coated carbon nanotube ring with enhanced raman scattering and photothermal conversion property for theranostic applications. J Am Chem Soc 2016;138(22):7005–15.
[57] Li D, Liu X, Li W, Lin ZH, Zhu B, Li ZZ, et al. Scalable and hierarchically designed polymer film as a selective thermal emitter for high-performance all-day radiative cooling. Nature Nanotech 2021;16(2):153–8.
[58] He Y, Lin X, Feng Y, Luo B, Liu M. Carbon nanotube ink dispersed by chitin nanocrystals for thermoelectric converter for self-powering multifunctional wearable electronics. Adv Sci (Weinh) 2022;9(33):2204675.